

KATRIN bound on 3+1 active-sterile neutrino mixing and the reactor antineutrino anomaly

C. Giunti,^{1,*} Y.F. Li,^{2,3,†} and Y.Y. Zhang^{2,3,‡}

¹*Istituto Nazionale di Fisica Nucleare (INFN), Sezione di Torino, Via P. Giuria 1, I-10125 Torino, Italy*

²*Institute of High Energy Physics, Chinese Academy of Sciences, Beijing 100049, China*

³*School of Physical Sciences, University of Chinese Academy of Sciences, Beijing 100049, China*
(Dated: 15 March 2020)

We present the bounds on 3+1 active-sterile neutrino mixing obtained from the first results of the KATRIN experiment. We show that the KATRIN data extend the Mainz and Troitsk bound to smaller values of Δm_{41}^2 for large mixing and improves the exclusion of the large- Δm_{41}^2 solution of the Huber-Muller reactor antineutrino anomaly. We also show that the combined bound of the Mainz, Troitsk, and KATRIN tritium experiments and the Bugey-3, NEOS, PROSPECT, and DANSS reactor spectral ratio measurements exclude most of the region in the $(\sin^2 2\vartheta_{ee}, \Delta m_{41}^2)$ plane allowed by the Huber-Muller reactor antineutrino anomaly. Considering two new calculations of the reactor neutrino fluxes, we show that one, that predicts a lower ^{235}U neutrino flux, is in agreement with the tritium and reactor spectral ratio measurements, whereas the other leads to a larger tension than the Huber-Muller prediction. We also show that the combined reactor spectral ratio and tritium measurements disfavor the Neutrino-4 indication of large active-sterile mixing. We finally discuss the constraints on the gallium neutrino anomaly.

I. INTRODUCTION

The KATRIN collaboration presented recently [1] the first results of their high-precision measurement of the electron spectrum from ^3H decay near the end point, where it is sensitive to neutrino masses at the eV level. They obtained an upper limit of 1.1 eV at 90% confidence level (CL) for the effective neutrino mass

$$m_\beta = \sqrt{\sum_{k=1}^3 |U_{ek}|^2 m_k^2}, \quad (1)$$

in the standard three-neutrino mixing framework, where U is the mixing matrix and m_k is the mass of the neutrino ν_k , with $k = 1, 2, 3$.

The KATRIN collaboration measured the electron spectrum down to $Q - 35$ eV, where $Q \simeq 18.57$ keV is the Q-value of ^3H , that corresponds to the end-point of the electron spectrum in the absence of neutrino mass effects. Using this spectral measurement, it is possible to constrain also the mixing with the electron neutrino of heavier non-standard neutrinos with masses smaller than about 35 eV. This is interesting in view of the indications in favor of the existence of such non-standard neutrinos given by the reactor antineutrino anomaly and the gallium neutrino anomaly (see the recent reviews in Refs. [2–4]). A possible explanation of these anomalies is short-baseline neutrino oscillations due to the existence of a non-standard neutrino with a mass of the order of 1 eV or larger. Since it is well established that there

are only three active flavor neutrinos, in the flavor basis the new neutrino must be sterile. This framework is commonly called 3+1 active-sterile neutrino mixing.

In this paper, we first calculate in Section II the upper bound on m_β in the standard framework of three-neutrino mixing, in order to test the validity of our analysis of the KATRIN data by comparing the results with those of the KATRIN collaboration. Then, in Section III, we calculate the KATRIN bounds on active-sterile neutrino mixing and we show that they are more stringent than those of the Mainz [5] and Troitsk [6, 7] experiments discussed in Ref. [8]. In Section IV, we compare the KATRIN bounds with the results of the 3+1 analysis of the reactor antineutrino anomaly [9] assuming the standard Huber-Muller reactor neutrino flux prediction [10, 11] and the two new predictions of Estienne, Fallot et al. [12] and Hayen, Kostensalo, Severijns, Suhonen [13]. In Section IV, we discuss also the bounds of experiments that measured the reactor antineutrino spectrum at different distances. In Section V, we compare the positive results of the Neutrino-4 reactor experiment [14] with the bounds from the tritium experiments and from the other reactor spectral ratio measurements. In Section VI, we discuss the constraints on the gallium neutrino anomaly. We finally summarize the results in Section VII.

II. THREE NEUTRINO MIXING

In this section we present the results of our analysis of the KATRIN data in the standard framework of three-neutrino mixing. This is useful in order to describe the method that we used in the analysis of the KATRIN data and in order to check its validity by comparing the results for m_β with those obtained by the KATRIN collaboration [1].

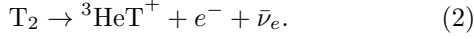
We consider the β -decay of the gaseous molecular tri-

* carlo.giunti@to.infn.it

† liyufeng@ihep.ac.cn

‡ zhangyiyu@ihep.ac.cn

tium source T_2 :



The differential electron spectrum is given by

$$R_\beta(E) = \frac{G_F^2 \cos^2 \theta_C}{2\pi^3} |\mathcal{M}|^2 F(E, Z+1) \\ \times (E + m_e) \sqrt{(E + m_e)^2 - m_e^2} \\ \times \sum_{i,j} |U_{ei}|^2 \zeta_j \varepsilon_j \sqrt{\varepsilon_j^2 - m_i^2} \Theta(\varepsilon_j - m_i), \quad (3)$$

where G_F is the Fermi constant, θ_C is the Cabibbo angle, \mathcal{M} is the nuclear matrix element, m_e is the electron mass, E is the kinetic energy of the outgoing electron, $F(E, Z+1)$ is the Fermi function describing the Coulomb effect of the electron, and $Z = 1$ is the atomic number of the parent nucleus. A fully relativistic description of the Fermi function is given by

$$F(E, Z) = 2(\gamma + 1) \frac{e^{\pi y}}{(2pR_n)^{2(1-\gamma)}} \frac{|\Gamma(\gamma + iy)|^2}{\Gamma(2\gamma + 1)^2}, \quad (4)$$

where $y = Z\alpha E/p$ and $\gamma = \sqrt{1 - \alpha^2 Z^2}$, with the fine-structure constant α and the complex Gamma function $\Gamma(z)$ [15]. The radius of the ${}^3\text{He}^{2+}$ nucleus is $R_n = 2.8840 \times 10^{-3}/m_e$ [16]. In Eq. (3), $\varepsilon_j = E_0 - E - V_j$ is the neutrino energy, with $E_0 = M_T - M_{3\text{He}} - m_e$, where M_T and $M_{3\text{He}}$ are, respectively, the mass of the initial and final nucleus. In the calculation of the β -decay electron spectrum $R_\beta(E)$, we considered the excitation states of the daughter molecular system, which have excitation energies V_j and a final-state distribution with probabilities ζ_j . These quantities are calculated with the Born-Oppenheimer approximation and can be found in Refs. [17, 18].

When the experimental resolution is much larger than the values of neutrino masses, one can define the effective neutrino mass m_β as in Eq. (1) and approximate the differential electron spectrum as

$$R_\beta(E) \simeq \frac{G_F^2 \cos^2 \theta_C}{2\pi^3} |\mathcal{M}|^2 F(E, Z+1) \\ \times (E + m_e) \sqrt{(E + m_e)^2 - m_e^2} \\ \times \sum_j \zeta_j \varepsilon_j \sqrt{\varepsilon_j^2 - m_\beta^2} \Theta(\varepsilon_j - m_\beta). \quad (5)$$

The KATRIN experiment combines a windowless gaseous molecular tritium source with a spectrometer based on the principle of magnetic adiabatic collimation with electrostatic filtering (MAC-E-filter) [19, 20]. This apparatus can measure the integral tritium β -spectrum

$$R(\langle qU \rangle) = R_{\text{bg}} + A_{\text{sig}} N_T \\ \times \int_{qU}^{E_0} R_\beta(E) f(E - \langle qU \rangle) dE, \quad (6)$$

which is the convolution of the differential β -decay electron spectrum $R_\beta(E)$ with the response function $f(E - \langle qU \rangle)$. N_T denotes the effective number of tritium atoms, R_{bg} is the energy-independent background rate and A_{sig} is the signal amplitude. The response function defines the probability of passing the MAC-E-filter for an electron with the kinetic energy E at the retarding potential energy qU . $\langle qU \rangle$ is the average over different pixels and scans and serves as the working variable of the integral electron spectrum. The response function used in our analysis is taken from the red curve of the top panel of Fig. 2 in Ref. [1]. Note that an energy resolution of 2.8 eV, which is determined by the energy filter width at the minimal and maximal magnetic fields, has been included in the response function. Moreover, an additional Gaussian smearing of 0.25 eV is also included to account for the average effect of $\langle qU \rangle$.

For the analysis of the KATRIN data, we considered the χ^2 function

$$\chi^2 = \sum_{i=1}^N \left(\frac{R_i^{\text{obs}} - R_i^{\text{pred}}(m_\beta^2 + \delta m_\beta^2)}{\sigma_i} \right)^2 + \left(\frac{\delta m_\beta^2}{0.32} \right)^2, \quad (7)$$

where R_i^{obs} and σ_i are the experimental rate and its statistical uncertainty corresponding to each retarding energy value $\langle qU \rangle_i$ in the upper panel of Fig. 3 in Ref. [1]. R_i^{pred} is the predicted rate calculated according to Eq. (6). The pull term for the variation δm_β^2 takes into account the systematic uncertainty of 0.32 eV^2 on m_β^2 given in Table I of Ref. [1]. In the fit we considered four free parameters: m_β^2 , the endpoint E_0 , the signal amplitude A_{sig} , and the background rate R_{bg} . We calculated the bounds for m_β^2 by marginalizing over E_0 , A_{sig} , and R_{bg} .

In Ref. [1], the KATRIN collaboration first analyzed the data allowing negative values of m_β^2 , as discussed in Ref. [21]. With this method, they obtained $m_\beta^2 = -1.0_{-1.1}^{+0.9} \text{ eV}^2$. Under the same assumption, we obtained $m_\beta^2 = -1.0 \pm 0.9 \text{ eV}^2$, which is approximately consistent with the official KATRIN result.

In order to calculate the upper bound on the absolute scale of neutrino masses in the framework of three-neutrino mixing, we considered only physical positive values of m_β^2 , as done by the KATRIN collaboration [1]. We obtained

$$m_\beta < 0.8 (0.9) \text{ eV} \quad \text{at } 90\% (95\%) \text{ CL}, \quad (8)$$

that nicely coincide with the bounds that the KATRIN collaboration obtained [1] using the Feldman-Cousins method [22].

The approximate agreement of our results for m_β in the standard framework of three-neutrino mixing with those of the KATRIN collaboration validates our analysis of the KATRIN data.

III. 3+1 STERILE NEUTRINO MIXING

After the successful test of our method of analysis of the KATRIN data in the case of three-neutrino mixing, we consider the extension to 3+1 active-sterile neutrino mixing with the differential electron spectrum

$$R_\beta(E) = (1 - |U_{e4}|^2) R_\beta(E, m_\beta) + |U_{e4}|^2 R_\beta(E, m_4), \quad (9)$$

where U is the 4×4 unitary mixing matrix, $R_\beta(E, m_\beta)$ is the three-neutrino differential electron spectrum in Eq. (5) with m_β redefined by¹

$$m_\beta^2 = \sum_{k=1}^3 \frac{|U_{ek}|^2}{1 - |U_{e4}|^2} m_k^2, \quad (10)$$

and $R_\beta(E, m_4)$ has the same expression with m_β replaced by m_4 . We will compare the results of our analysis of the KATRIN data with the results of short-baseline (SBL) reactor neutrino oscillation experiments, that probe the effective SBL survival probability

$$P_{\nu_e \rightarrow \nu_e}^{\text{SBL}(-)} = 1 - \sin^2 2\vartheta_{ee} \sin^2 \left(\frac{\Delta m_{41}^2 L}{4E} \right), \quad (11)$$

where $\Delta m_{ij}^2 = m_i^2 - m_j^2$, $\sin^2 2\vartheta_{ee} = 4|U_{e4}|^2(1 - |U_{e4}|^2)$, L is the source-detector distance, and E is the neutrino energy. Note that neutrino oscillation experiments are sensitive to the squared-mass difference² $\Delta m_{41}^2 \simeq \Delta m_{42}^2 \simeq \Delta m_{43}^2$, whereas the KATRIN experiment is sensitive to m_β and m_4 . Therefore, in order to compare the respective results one must make some assumption on the value of one of the three light neutrino masses (m_1, m_2, m_3), that fixes the value of m_β through the precise knowledge of the values of the three-neutrino mixing parameters obtained by global fits of solar, atmospheric and long-baseline neutrino oscillation data [23–26]:

$$\Delta m_{21}^2 \simeq 7.5 \times 10^{-5} \text{ eV}^2, \quad (12)$$

$$|\Delta m_{31}^2| \simeq |\Delta m_{32}^2| \simeq 2.5 \times 10^{-3} \text{ eV}^2, \quad (13)$$

$$|U_{e2}|^2 \simeq 0.3, \quad (14)$$

$$|U_{e3}|^2 \simeq 0.022, \quad (15)$$

with positive and negative $\Delta m_{31}^2 \simeq \Delta m_{32}^2$ in the two possible cases of Normal Ordering (NO) and Inverted Ordering (IO) of the three light neutrino masses, respectively

(see the recent review in Ref. [27]). Equation (10) can be written as

$$m_\beta^2 = m_1^2 + \frac{|U_{e2}|^2 \Delta m_{21}^2 + |U_{e3}|^2 \Delta m_{31}^2}{1 - |U_{e4}|^2}. \quad (16)$$

Hence, we have

$$\text{NO: } m_\beta^2 \simeq m_1^2 + \frac{7.8 \times 10^{-5} \text{ eV}^2}{1 - |U_{e4}|^2}, \quad (17)$$

$$\text{IO: } m_\beta^2 \simeq m_1^2 - \frac{3.3 \times 10^{-5} \text{ eV}^2}{1 - |U_{e4}|^2}. \quad (18)$$

Therefore, taking into account that the sensitivity of KATRIN to m_β^2 is at the level of the eV^2 and considering³ $|U_{e4}|^2 < 0.5$ for $\sin^2 2\vartheta_{ee} < 1$, we can neglect the small deviations of m_β^2 from m_1^2 in Eqs. (17) and (18), and consider the approximate relation

$$\Delta m_{41}^2 \simeq m_4^2 - m_\beta^2. \quad (19)$$

We performed two analyses of the KATRIN data in the framework of 3+1 active-sterile neutrino mixing. First, we fitted the data considering $A_{\text{sig}}, R_{\text{bg}}, E_0, m_\beta, |U_{e4}|^2$, and m_4 as free parameters and we calculated the “free m_β ” confidence level contours in the $(\sin^2 2\vartheta_{ee}, \Delta m_{41}^2)$ plane shown in Figure 1 marginalizing the χ^2 over $A_{\text{sig}}, R_{\text{bg}}, E_0$ and m_β . This is the most general bound on 3+1 mixing given by the KATRIN data. We also calculated the confidence level contours in the case of a negligible m_β , shown by the $m_\beta = 0$ lines in Figure 1. This is a reasonable assumption motivated by the likeliness of a neutrino mass hierarchy, with $m_{1,2,3} \ll m_4$. It is also useful for the comparison in Figure 1 of the KATRIN bounds with the exclusion curves of the Mainz [5] and Troitsk [6, 7] experiments obtained in Ref. [8] under the same assumption. One can see from Figure 1 that the KATRIN bounds obtained with free m_β and $m_\beta = 0$ are slightly different only around $\Delta m_{41}^2 \approx 200 - 300 \text{ eV}^2$, where the Mainz+Troitsk bound is dominant. Therefore, in the following we can safely consider only the analysis of KATRIN data with $m_\beta = 0$.

Figure 1 shows that the analysis of the KATRIN data yields a 1σ allowed region with non-zero active-sterile neutrino mixing around the best-fit point at $\sin^2 2\vartheta_{ee} = 0.046$ and $\Delta m_{41}^2 = 257 \text{ eV}^2$. Since the 1σ KATRIN allowed region is in tension with the Mainz+Troitsk bound, it is likely due to a statistical fluctuation. Therefore, in the following we will consider only the KATRIN exclusion curves at higher confidence level. However, the slight tension between KATRIN and Mainz+Troitsk has effects on the combined bound that will be discussed below.

Figure 1 shows that the KATRIN data allow us to extend the Mainz+Troitsk excluded region at large mixing

¹ The necessity of the factor $(1 - |U_{e4}|^2)$ in front of $R_\beta(E, m_\beta)$ can be understood by noting that in the limit of negligible masses of ν_1, ν_2 , and ν_3 , their contribution to the electron spectrum is given by Eq. (3) with $m_1 = m_2 = m_3 = 0$. In this case one can extract a common mixing factor $\sum_{i=1}^3 |U_{ei}|^2 = 1 - |U_{e4}|^2$ and write the contribution of ν_1, ν_2 , and ν_3 as $(1 - |U_{e4}|^2) R_\beta(E, 0)$.

² The effective SBL survival probability (11) is derived under the approximation $\Delta m_{41}^2 \simeq \Delta m_{42}^2 \simeq \Delta m_{43}^2 \gtrsim 0.1 \text{ eV}^2$, taking into account the smallness of the values of Δm_{21}^2 and $|\Delta m_{31}^2| \simeq |\Delta m_{32}^2|$, given in Eqs. (12) and (13), respectively.

³ Since 3+1 active-sterile neutrino mixing is allowed only as a perturbation of standard three-neutrino mixing, $|U_{e4}|^2$ cannot be large (see the recent reviews in Refs. [2–4]).

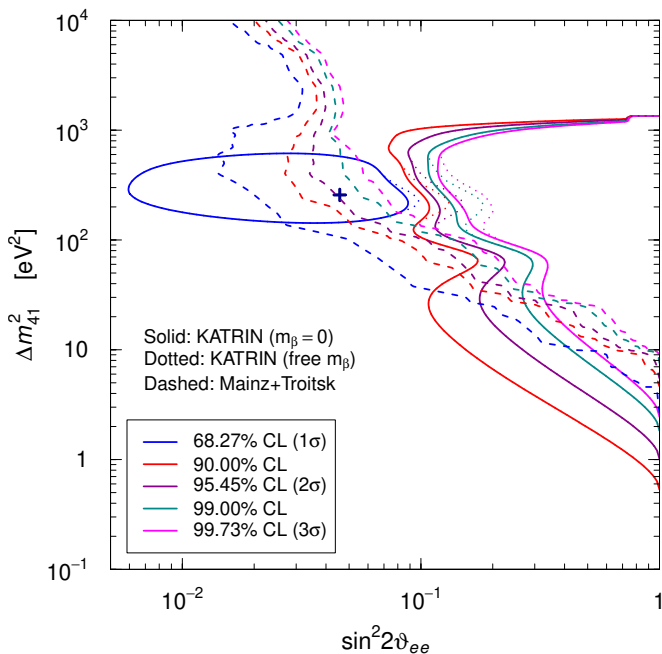


FIG. 1. Confidence level contours in the $(\sin^2 2\vartheta_{ee}, \Delta m_{41}^2)$ plane obtained from the analysis of KATRIN data with $m_\beta = 0$ (solid) and free m_β (dotted), and from the results of the Mainz [5] and Troitsk [6, 7] experiments [8]. The blue cross indicates the KATRIN best-fit point.

to smaller value of Δm_{41}^2 , reaching the interesting values of Δm_{41}^2 below 10 eV^2 . In the logarithmic scale of Figure 1, the KATRIN bounds on $\sin^2 2\vartheta_{ee}$ have an approximately linear decrease when Δm_{41}^2 increases from about 6 eV^2 to about 30 eV^2 , that corresponds to $m_4 \approx 5.5 \text{ eV}$. For larger values of Δm_{41}^2 , the effect of ν_4 on the electron spectrum occurs at a distance from the end point for which the data are less constraining. This leads to oscillations of the bounds from $\Delta m_{41}^2 \approx 30 \text{ eV}^2$ to $\Delta m_{41}^2 \approx 10^3 \text{ eV}^2$, that corresponds to the value $m_4 \approx 32 \text{ eV}$ for which the data become completely ineffective.

Figure 2 shows the combined 90% and 99% CL bounds of the tritium experiments compared with the corresponding KATRIN and Mainz+Troitsk bounds (and the regions allowed by the reactor antineutrino anomaly to be discussed in Section IV). One can see that the combined tritium bound extends the Mainz+Troitsk excluded region at large mixing to values of Δm_{41}^2 below 10 eV^2 . However, the combined tritium bound is less stringent than the KATRIN bound in the small- Δm_{41}^2 range where the KATRIN data are dominant (this occurs much more for the 90% CL bound than for the 99% CL bound). This strange behavior is due to the location of the minimum of the KATRIN χ^2 , that is shown in Figure 2 by the blue cross, in a point where the Mainz+Troitsk χ^2 is not small. The location of the minimum χ^2 of the combined fit is shown in Figure 2 by the red cross and it is obviously larger than the KATRIN χ^2 minimum ($\Delta\chi^2 = 2.5$), since it lies out of the KATRIN 1σ allowed region shown in

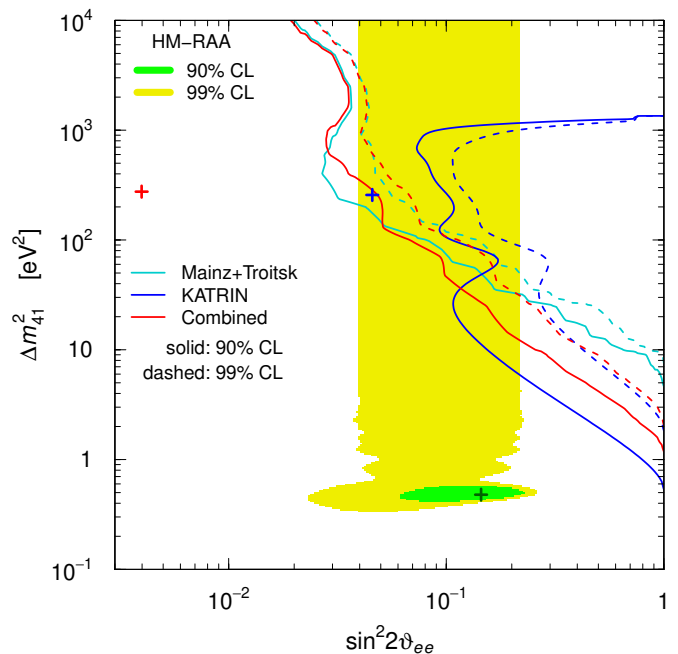


FIG. 2. 90% and 99% CL exclusion curves in the $(\sin^2 2\vartheta_{ee}, \Delta m_{41}^2)$ plane obtained from the analysis of KATRIN data with free m_β and $m_\beta = 0$. Also shown are the exclusion curves of the Mainz [5] and Troitsk [6, 7] experiments obtained in Ref. [8] and the combined exclusion curves. The green and yellow regions are allowed at 90% and 99% CL by the neutrino oscillation solution [28] of the Huber-Muller reactor antineutrino anomaly (HM-RAA). The crosses indicate the best-fit points.

Fig. 1. Since the confidence level contours are determined by the difference of χ^2 (given by Table 39.2 of Ref. [26] for two degrees of freedom) with respect to the minimum corresponding to the chosen confidence level, the increase of the χ^2 minimum leads to a shift towards larger values of $\sin^2 2\vartheta_{ee}$ of the combined tritium bound with respect to the KATRIN bound in the Δm_{41}^2 range where KATRIN is dominant. For a similar reason, the combined tritium bound is less stringent than the Mainz+Troitsk bound for $\Delta m_{41}^2 \approx 100 - 600 \text{ eV}^2$, where the Mainz+Troitsk bound is dominant.

IV. THE REACTOR ANTINEUTRINO ANOMALY

In Figure 2 we have also drawn the regions allowed by the reactor antineutrino anomaly (HM-RAA) [9] according to the recent analysis in Ref. [28] of reactor antineutrino data compared with the Huber-Muller prediction [10, 11] (see also Ref. [29]). One can see that the combined constraints of tritium-decay experiments can exclude the large- Δm_{41}^2 part of the RAA 99% allowed region, but it is still too weak to affect the 90% allowed region around the best-fit point. Note that this HM-RAA region is different from the original reactor antineutrino

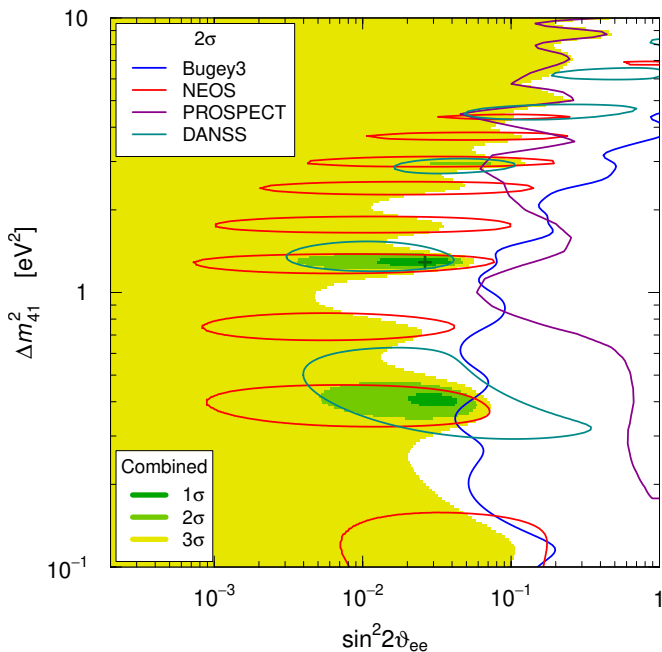


FIG. 3. Contours of the 2σ regions in the $(\sin^2 2\vartheta_{ee}, \Delta m_{41}^2)$ plane obtained from the reactor spectral ratio measurements of the Bugey-3, NEOS, PROSPECT and DANSS experiments. The shadowed regions are allowed by the combined fit, with the best fit point indicated by the cross.

anomaly allowed region in Ref. [9] (see also Ref. [30]) mainly because it takes into account only the measured reactor neutrino rates, without the Bugey-3 [31] 14 m / 15 m spectral ratio that were included in Refs. [9, 30]. As nicely illustrated in Fig. 1 of Ref. [32], the Bugey-3 spectral ratio excludes large mixing for $\Delta m_{41}^2 \lesssim 2 \text{ eV}^2$, moving the best-fit region from $\Delta m_{41}^2 \approx 0.5 \text{ eV}^2$ to $\Delta m_{41}^2 \approx 1.8 \text{ eV}^2$. However, in discussing the reactor antineutrino anomaly it is better to separate the model-dependent anomaly based on the absolute neutrino rate measurements and the model-independent implications of the spectral-ratio measurements.

Recently, also the new reactor neutrino experiments DANSS [33, 34], PROSPECT [35], and STEREO [36, 37] measured the reactor antineutrino spectrum at different distances. Moreover, the NEOS [38] experiments presented the results of a measurement of the reactor antineutrino spectrum at 24 m from a reactor, relative to the spectrum measured at about 500 m by the Daya Bay near detectors [39]. These measurements provide information on short-baseline neutrino oscillations that are independent of the theoretical calculation of the reactor antineutrino flux. Therefore, they can test the model-dependent reactor antineutrino anomaly and their results can be combined with the bounds given by the tritium experiments. Here we consider the published results of the Bugey-3 [31], NEOS [38], and PROSPECT [35] experiments, together with the preliminary 2019 results of the DANSS [34] experiment, that improve significantly the published 2018 results [34]. We cannot include in

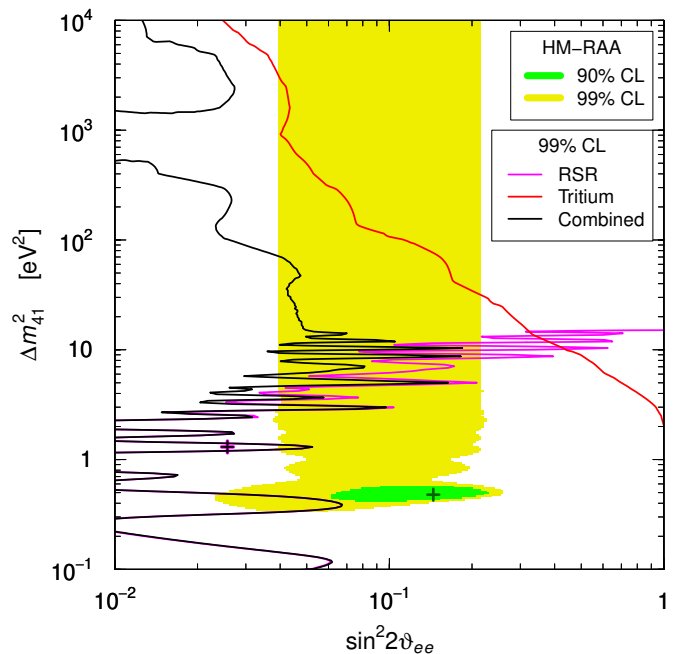


FIG. 4. 99% CL exclusion curves in the $(\sin^2 2\vartheta_{ee}, \Delta m_{41}^2)$ plane obtained from the analysis of the data of the Mainz, Troitsk and KATRIN tritium experiments and the combined analysis of the reactor spectral ratio (RSR) measurements of the Bugey-3, NEOS, PROSPECT and DANSS experiments. Also shown is the combined tritium and reactor spectral-ratio exclusion curve and the regions allowed at 90% and 99% CL by the neutrino oscillation solution [28] of the Huber-Muller reactor antineutrino anomaly (HM-RAA). The crosses indicate the best-fit points.

the analysis the results of the STEREO [36, 37] experiment, because there is not enough available information. For the Bugey-3 experiment we used the same analysis that we used in previous papers [28, 40, 41]. For the NEOS experiment we use the χ^2 table kindly provided by the NEOS collaboration. For the PROSPECT experiment we use the χ^2 table published as ‘‘Supplemental Material’’ of Ref. [35]. For the DANSS experiment we performed an approximate least-square analysis of the 2019 data presented in Fig. 5 of Ref. [34] that reproduces approximately the DANSS exclusion curves in Fig. 6 of the same paper.

Figure 3 shows the contours of the 2σ regions in the $(\sin^2 2\vartheta_{ee}, \Delta m_{41}^2)$ plane obtained from the reactor spectral ratio measurements of the Bugey-3, NEOS, PROSPECT and DANSS experiments, and the regions allowed at 1σ , 2σ , and 3σ by the combined fit. One can see that there is an indication in favor of short-baseline oscillations at the level of about 2σ , that is due to the coincidence of the NEOS and DANSS allowed regions at $\Delta m_{41}^2 \approx 1.3 \text{ eV}^2$, where there is the best-fit point of the combined fit for $\sin^2 2\vartheta_{ee} = 0.026$ and $\Delta m_{41}^2 = 1.3 \text{ eV}^2$. The NEOS and DANSS allowed regions partially overlap also at $\Delta m_{41}^2 \approx 0.4 \text{ eV}^2$, where there is a combined 1σ -allowed region, and at $\Delta m_{41}^2 \approx 3 \text{ eV}^2$, where

there is a tiny combined 2σ -allowed region. This model-independent indication in favor of short-baseline oscillations was discussed in Refs. [41, 42] using the 2018 [33] DANSS data and in Ref. [29] using both the 2018 and the 2019 [34] DANSS data. Here, as explained above, we use the 2019 DANSS data, that lead to a diminished indication in favor of short-baseline oscillations with respect to the 2018 DANSS data. Indeed, from the combined NEOS and DANSS analyses we find only a 2.6σ indication of short-baseline oscillations, that is smaller than the 3.7σ obtained in Ref. [41]. These values agree approximately with those found in Ref. [29].

Figure 4 shows the 99% exclusion curve in the $(\sin^2 2\vartheta_{ee}, \Delta m_{41}^2)$ plane obtained from the combined analysis of the Bugey-3, NEOS, PROSPECT and DANSS spectral ratios, that constrain the mixing for low values of Δm_{41}^2 , together with the combined 99% CL exclusion curve of the Mainz, Troitsk and KATRIN tritium experiments, that constrains the mixing for large values of Δm_{41}^2 . Figure 4 shows also the combined tritium and reactor spectral-ratio 99% CL exclusion curve, that disfavors most of the 99% CL allowed region [28] of the Huber-Muller reactor antineutrino anomaly. Note that the combined tritium and reactor spectral-ratio bound at large values of Δm_{41}^2 is much more stringent than the tritium bound, in spite of the lack of sensitivity of the reactor spectral ratio experiments for $\Delta m_{41}^2 \gtrsim 10 \text{ eV}^2$. The reason is that the 99% exclusion curve is determined by the appropriate difference of χ^2 (given by Table 39.2 of Ref. [26] for two degrees of freedom) with respect to the global χ^2 minimum that occurs at $\sin^2 2\vartheta_{ee} = 0.026$ and $\Delta m_{41}^2 = 1.3 \text{ eV}^2$. This point practically coincides with the reactor spectral ratio best fit in Figure 3 and is far away from the tritium-only best fit in Figure 2, because the reactor spectral ratio data are dominant in the combined fit. The stringent combined tritium and reactor spectral-ratio bound at large values of Δm_{41}^2 is due to the combined effects of the tritium bound in that region and the reactor spectral ratio data that allow these large values of Δm_{41}^2 only at 3σ , as can be seen in Figure 3. The reactor spectral ratio data χ^2 has this effect for large values of Δm_{41}^2 , where the experiments are not sensitive, because the data prefer the small- Δm_{41}^2 region near the best fit. This is an obviously correct effect if one thinks that the measurement of a physical quantity in an experiment excludes all the values of the physical quantity that are enormously different from the measured one and for which the experiment is not sensitive.

Figure 4 shows that there is a tension between the active-sterile oscillations indicated by the Huber-Muller reactor antineutrino anomaly and the combined bound obtained from tritium and reactor spectral-ratio measurements. However, it is likely that the Huber-Muller neutrino flux prediction must be revised, as indicated by the observation of a large spectral distortion at 5 MeV in the RENO [43, 44], Double Chooz [45], Daya Bay [39], and NEOS [38] experiments (see the reviews in Refs. [46, 47]). As already discussed in Ref. [29], there

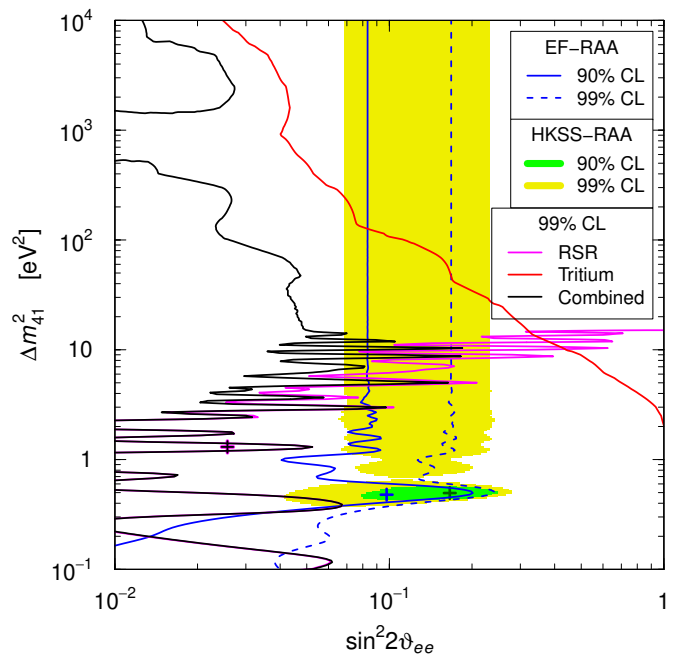


FIG. 5. 99% CL exclusion curves in the $(\sin^2 2\vartheta_{ee}, \Delta m_{41}^2)$ plane obtained from the combined analysis of the data of the Mainz, Troitsk and KATRIN tritium experiments and the combined analysis of the reactor spectral ratio (RSR) measurements of the Bugey-3, NEOS, PROSPECT and DANSS experiments. Also shown is the combined tritium and reactor spectral-ratio exclusion curve and the regions allowed at 90% and 99% CL by the fits of the absolute reactor rates assuming the Estienne, Fallot et al. [12] (EF-RAA) and the Hayen, Kostensalo, Severijns, Suhonen [13] (HKSS-RAA) reactor neutrino fluxes. The crosses indicate the best-fit points.

are two recent reactor neutrino flux calculations that may improve the Huber-Muller prediction: the calculation of Estienne, Fallot et al. (EF) [12] that is based on the summation method, and the calculation of Hayen, Kostensalo, Severijns, Suhonen (HKSS) [13] that improves the conversion method by including the effects of forbidden β decays through shell-model calculations. Unfortunately, as discussed in Ref. [29], a comparison of the results of the two new calculations does not lead to a clarification of the problem of the reactor antineutrino anomaly, because the corresponding neutrino flux predictions diverge: the EF calculation resulted in a ^{235}U neutrino flux prediction that is smaller than the HM prediction, leading to a decrease of the reactor antineutrino anomaly, whereas the HKSS fluxes are larger than the HM fluxes, leading to an increase of the reactor antineutrino anomaly. Figure 5 show a comparison of the bounds in the $(\sin^2 2\vartheta_{ee}, \Delta m_{41}^2)$ plane obtained from the tritium experiments and the reactor spectral ratios with the regions allowed by the fits of the absolute reactor rates assuming the EF and HKSS fluxes. We took into account the uncertainties of the HKSS fluxes given in Ref. [13]. On the other hand, since the EF cross section per fission are given in Ref. [12] without the associated uncertainties, for them we adopted the

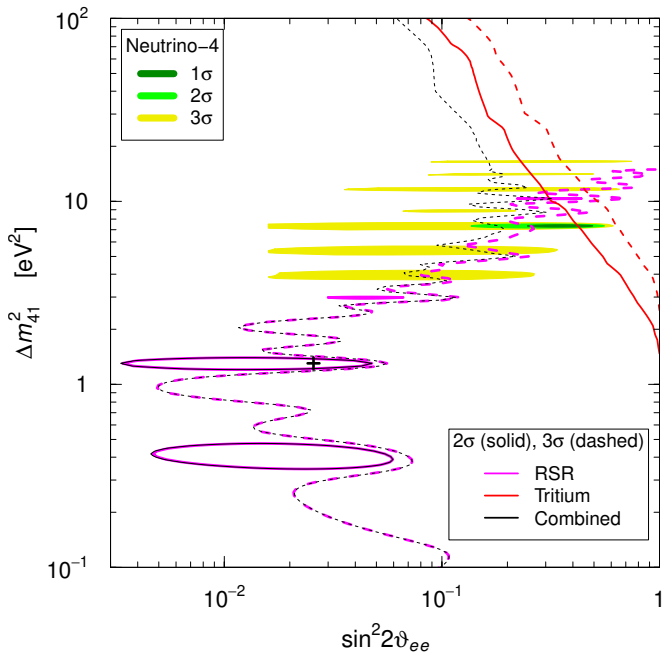


FIG. 6. 2σ and 3σ bounds in the $(\sin^2 2\vartheta_{ee}, \Delta m_{41}^2)$ plane obtained from the combined analysis of the data of the Mainz, Troitsk and KATRIN tritium experiments and the combined analysis of the reactor spectral ratio (RSR) measurements of the Bugey-3, NEOS, PROSPECT and DANSS experiments. Also shown are the combined tritium and reactor spectral-ratio bounds (with the best fit indicated by the black cross) and the regions allowed at 1σ , 2σ , and 3σ by the results of the Neutrino-4 reactor experiment [14].

uncertainties associated with the summation spectra estimated in Ref. [48]: 5% for ^{235}U , ^{239}Pu , and ^{241}Pu , and 10% for ^{238}U .

From Figure 5, one can see that the EF neutrino flux calculation leads only to an upper bound on the mixing at 90% CL and higher. Therefore, in this case the reactor antineutrino anomaly is not statistically significant and the EF-RAA upper bound is compatible with the upper bounds obtained from the tritium experiments and the reactor spectral ratios.

On the other hand, the HKSS fluxes lead to an increase of the reactor antineutrino anomaly with respect to the HM prediction and the corresponding HKSS-RAA allowed regions in Figure 5 are limited to larger mixing than the HM-RAA allowed regions in Figure 4. Therefore, the tension of the HKSS-RAA with the tritium and reactor spectral ratios bounds is larger than that of the HM-RAA. From Figure 5 one can see that only very small portions of the HKSS-RAA 99% allowed region are not excluded by the combined 99% bound of the tritium experiments and the reactor spectral ratios.

V. NEUTRINO-4

Let us now consider the results of the Neutrino-4 reactor experiment [14], that is another experiment that measured the ratios of the spectra at different distances from the reactor, between 6 and 12 m. We did not consider it so far because the result of this experiment is an anomalous indication of short-baseline oscillations with large mixing that is in tension with all the other experimental results. This can be seen in Figure 6, where we compare the bounds in the $(\sin^2 2\vartheta_{ee}, \Delta m_{41}^2)$ plane obtained from the tritium experiments and the reactor spectral ratios with the allowed regions of the Neutrino-4 reactor experiment [14]. One can see that the large-mixing parts of the Neutrino-4 allowed regions are excluded by the 3σ combined tritium and reactor spectral-ratio exclusion curve.

At 2σ , the combination of the reactor spectral-ratio and tritium measurements have allowed regions at $\Delta m_{41}^2 \approx 1.3 \text{ eV}^2$, where there is the best-fit point for $\sin^2 2\vartheta_{ee} = 0.026$ and $\Delta m_{41}^2 = 1.3 \text{ eV}^2$, and at $\Delta m_{41}^2 \approx 0.4 \text{ eV}^2$, that correspond to those in Figure 3 and are due to the coincidence of the NEOS and DANSS allowed regions discussed above. Therefore, all the 3σ Neutrino-4 allowed regions are excluded at 2σ by the reactor spectral-ratio and tritium measurements.

Moreover, the large- $\sin^2 2\vartheta_{ee}$ parts of the 3σ Neutrino-4 allowed regions and most of the 2σ Neutrino-4 allowed region are excluded by the combined 3σ tritium and reactor spectral ratio bound.

VI. THE GALLIUM NEUTRINO ANOMALY

Let us finally consider the gallium neutrino anomaly [30, 52–58], that is a short-baseline disappearance of ν_e 's found in the gallium radioactive source experiments GALLEX [59–61] and SAGE [53, 62–64]. There is some uncertainty on the magnitude of the gallium neutrino anomaly, that depends on the detection cross section, which must be calculated, as in Refs. [50, 52], or extrapolated from measurements of (p, n) [49, 65] or $(^3\text{He}, ^3\text{H})$ [51] charge-exchange reactions. Figure 7 shows the regions in the $(\sin^2 2\vartheta_{ee}, \Delta m_{41}^2)$ plane allowed at 90% CL by the gallium neutrino anomaly using the detection cross sections considered recently in Ref. [52], where a new shell model calculation based on the effective Hamiltonian JUN45 was presented. The Bahcall cross section was derived in Ref. [49] from the (p, n) charge-exchange measurements in Ref. [65]. The Haxton cross section was calculated in Ref. [50] using a shell model. The Frekers cross section was obtained from the $(^3\text{He}, ^3\text{H})$ [51] charge-exchange measurements in Ref. [51].

As done in Ref. [52], we show in Figure 7 the contours of the 90% CL allowed regions that have a lower bound for the effective mixing parameter $\sin^2 2\vartheta_{ee}$. One can see that the relatively large Haxton cross section gives

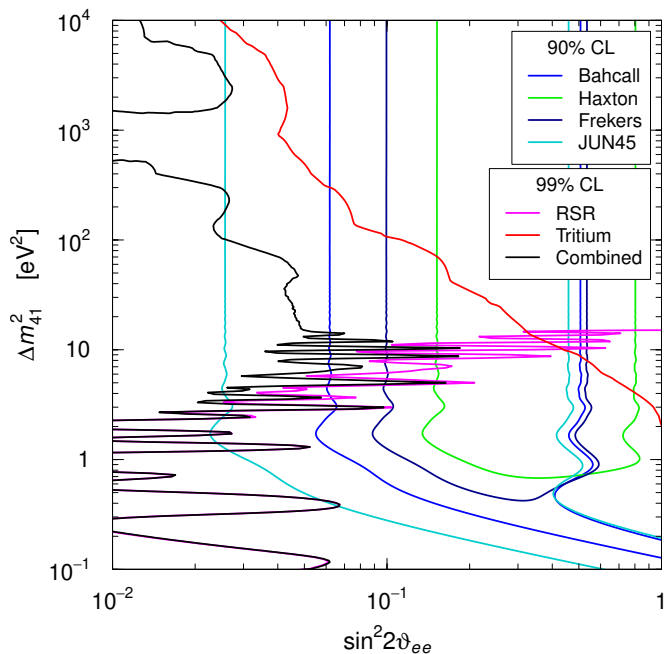


FIG. 7. Comparison of the regions in the $(\sin^2 2\vartheta_{ee}, \Delta m_{41}^2)$ plane allowed at 90% CL by the gallium neutrino anomaly using the Bahcall [49], Haxton [50], Frekers [51], and JUN45 [52] neutrino detection cross sections discussed in Ref. [52] with the 99% CL exclusion curves obtained from the combined analysis of the data of the Mainz, Troitsk and KATRIN tritium experiments and the combined analysis of the reactor spectral ratio (RSR) measurements of the Bugey-3, NEOS, PROSPECT and DANSS experiments. Also shown is the combined tritium and reactor exclusion curve.

the strongest anomaly, which requires rather large active sterile mixing and is in severe tension with the tritium and reactor spectral ratio bounds. Almost all the 90% CL Haxton allowed region is excluded at 99% CL by the combined tritium and reactor spectral ratio bound. The smaller Frekers and Bahcall cross sections allow smaller values of the mixing, but the corresponding 90% CL allowed regions in Figure 7 are in tension with the combined tritium and reactor spectral ratio 99% CL exclusion curve, with only some very small not-excluded areas. The JUN45 cross section is the smallest one and allows the smallest mixing, as one can see from Figure 7, where the corresponding 90% CL allowed region has several areas that are not excluded by the combined 99% CL tritium and reactor spectral ratio bound. In particular, there is a large not-excluded area at large values of Δm_{41}^2 , between about 5 and 100 eV^2 . These comparisons indicate that the smallest JUN45 gallium detection cross section is favored with respect to the others. Note that the KATRIN bound is essential for the exclusion of large parts of the gallium allowed regions for Δm_{41}^2 between about 10 and 80 eV^2 , where the KATRIN data dominate the tritium bound.

VII. CONCLUSIONS

In this paper we have discussed the implications for 3+1 active-sterile neutrino mixing of the recent KATRIN data [1] on the search for the absolute value of neutrino masses. We have first analyzed the KATRIN data in the framework of standard three-neutrino mixing, in order to check the validity of our method by comparing the resulting bound on the effective mass m_β with that obtained by the KATRIN collaboration. Then, we have presented the bounds obtained from the analysis of the KATRIN data on the short-baseline oscillation parameters $\sin^2 2\vartheta_{ee}$ and Δm_{41}^2 in the framework of 3+1 active-sterile neutrino mixing. We have shown that the KATRIN data allow to improve the bounds of the Mainz [5] and Troitsk [6, 7] experiments discussed in Ref. [8] extending the excluded region from $\Delta m_{41}^2 \approx 10 - 100 \text{eV}^2$ to $\Delta m_{41}^2 \approx 1 - 10 \text{eV}^2$ for large mixing ($\sin^2 2\vartheta_{ee} \gtrsim 0.1$). This result allows us to extend the exclusion of the large- Δm_{41}^2 solution of the Huber-Muller reactor antineutrino anomaly to $\Delta m_{41}^2 \approx 10 \text{eV}^2$ for $\sin^2 2\vartheta_{ee} \approx 0.1$ at 90% CL (see Figure 2).

We also considered the model-independent bounds of the Bugey-3 [31], NEOS [38], PROSPECT [35], and DANSS [33, 34] experiments that measured the reactor antineutrino spectrum at different distances. We have shown that there is a persistent model-independent indication [29, 41, 42] of short-baseline oscillations due to the coincidence of the NEOS and DANSS allowed regions, albeit with a smaller statistical significance passing from the 2018 [33] to the 2019 [34] DANSS data, in agreement with the discussion in Ref. [29].

The combination of the bounds of the reactor spectral ratio measurements exclude most of the low- Δm_{41}^2 solution of the Huber-Muller reactor antineutrino anomaly. Therefore, combining the tritium and reactor spectral ratio bounds, we are able to exclude most of the region in the $(\sin^2 2\vartheta_{ee}, \Delta m_{41}^2)$ plane corresponding to the short-baseline solution of the Huber-Muller reactor antineutrino anomaly (see Figure 4).

We also discussed the implications of these bounds for the interpretations of the absolute reactor antineutrino rates assuming one of the two recent new reactor neutrino flux calculations by Estienne, Fallot et al. (EF) [12] and Hayen, Kostensalo, Severijns, Suhonen (HKSS) [13]. We have shown that the EF calculation, that predicts a ^{235}U neutrino flux that is smaller than that of Huber-Muller, is in agreement with the bounds on 3+1 mixing obtained from the tritium and reactor spectral ratio measurements. On the other hand, since the HKSS calculation predicts reactor neutrino fluxes that are larger than those of Huber-Muller, the HKSS antineutrino anomaly region in the $(\sin^2 2\vartheta_{ee}, \Delta m_{41}^2)$ plane is more excluded than the Huber-Muller one (see Figure 5).

We also compared the tritium and reactor spectral ratio bounds on 3+1 mixing with the indication of large mixing of the Neutrino-4 reactor experiment [14]. We have shown that the Neutrino-4 allowed regions in the

($\sin^2 2\theta_{ee}, \Delta m_{41}^2$) plane are excluded at 2σ by the other reactor spectral ratio measurements. The 3σ combined tritium and reactor spectral ratio bound excludes the large- $\sin^2 2\theta_{ee}$ parts of the 3σ Neutrino-4 allowed regions. (see Figure 6).

We finally considered the gallium neutrino anomaly and we have shown that the combined bound of tritium and reactor spectral ratio measurements favor the recent JUN45 shell model calculation of the neutrino-gallium cross section [52] with respect to older estimates [49–51].

ACKNOWLEDGMENTS

We would like to thank Bryce Littlejohn, Loredana Gastaldo and Francesco Vissani for useful discussions that helped to improve the paper. The work of C. Giunti was partially supported by the research grant "The Dark Universe: A Synergic Multimessenger Approach" number 2017X7X85K under the program PRIN 2017 funded by the Ministero dell'Istruzione, Università e della Ricerca (MIUR). The work of Y.F. Li and Y.Y. Zhang was supported in part by Beijing Natural Science Foundation under Grant No. 1192019, and by the National Natural Science Foundation of China under Grant No. 11835013. Y.F. Li is also grateful for the support by the CAS Center for Excellence in Particle Physics (CCEPP).

-
- [1] M. Aker *et al.* (KATRIN), *Phys.Rev.Lett.* **123**, 221802 (2019), arXiv:1909.06048 [hep-ex].
- [2] C. Giunti and T. Lasserre, *Ann. Rev. Nucl. Part. Sci.* **69**, 163 (2019), arXiv:1901.08330 [hep-ph].
- [3] A. Diaz, C. Argüelles, G. Collin, J. Conrad, and M. Shaevitz, arXiv:1906.00045 [hep-ex].
- [4] S. Boser, C. Buck, C. Giunti, J. Lesgourgues, L. Ludhova, S. Mertens, A. Schukraft, and M. Wurm, *Prog.Part.Nucl.Phys.* **111**, 103736 (2020), arXiv:1906.01739 [hep-ex].
- [5] C. Kraus, A. Singer, K. Valerius, and C. Weinheimer, *Eur.Phys.J.* **C73**, 2323 (2013), arXiv:1210.4194 [hep-ex].
- [6] A. Belesev, A. Berlev, E. Geraskin, A. Golubev, N. Likhovid, *et al.*, *JETP Lett.* **97**, 67 (2013), arXiv:1211.7193 [hep-ex].
- [7] A. Belesev *et al.*, *J. Phys.* **G41**, 015001 (2014), arXiv:1307.5687 [hep-ex].
- [8] C. Giunti, M. Laveder, Y. F. Li, and H. Long, *Phys. Rev.* **D87**, 013004 (2013), arXiv:1212.3805 [hep-ph].
- [9] G. Mention *et al.*, *Phys. Rev.* **D83**, 073006 (2011), arXiv:1101.2755 [hep-ex].
- [10] T. A. Mueller *et al.*, *Phys. Rev.* **C83**, 054615 (2011), arXiv:1101.2663 [hep-ex].
- [11] P. Huber, *Phys. Rev.* **C84**, 024617 (2011), arXiv:1106.0687 [hep-ph].
- [12] M. Estienne, M. Fallot, *et al.*, *Phys. Rev. Lett.* **123**, 022502 (2019), arXiv:1904.09358 [nucl-ex].
- [13] L. Hayen, J. Kostensalo, N. Severijns, and J. Suhonen, *Phys.Rev.* **C100**, 054323 (2019), arXiv:1908.08302 [nucl-th].
- [14] A. Serebrov *et al.* (Neutrino-4), *Pisma Zh.Eksp.Teor.Fiz.* **109**, 209 (2019), arXiv:1809.10561 [hep-ex].
- [15] E. J. Konopinski and G. E. Uhlenbeck, *Phys. Rev.* **48**, 7 (1935).
- [16] P. O. Ludl and W. Rodejohann, *JHEP* **1606**, 040 (2016), arXiv:1603.08690 [hep-ph].
- [17] A. Saenz, S. Jonsell, and P. Froelich, *Phys. Rev. Lett.* **84**, 242 (2000).
- [18] N. Doss, J. Tennyson, A. Saenz, and S. Jonsell, *Phys. Rev.* **C73**, 025502 (2006).
- [19] V. M. Lobashev and P. E. Spivak, *Nucl. Instrum. Meth.* **A240**, 305 (1985).
- [20] A. Picard, H. Backe, H. Barth, J. Bonn, B. Degen, T. Edling, R. Haid, A. Hermanni, P. Leiderer, T. Loeken, A. Molz, R. Moore, A. Osipowicz, E. Otten, M. Przyrembel, M. Schrader, M. Steininger, and C. Weinheimer, *Nuclear Instruments and Methods in Physics Research Section B: Beam Interactions with Materials and Atoms* **63**, 345 (1992).
- [21] M. Kleesiek *et al.*, *Eur.Phys.J.* **C79**, 204 (2019), arXiv:1806.00369 [physics].
- [22] G. J. Feldman and R. D. Cousins, *Phys. Rev.* **D57**, 3873 (1998), physics/9711021.
- [23] P. F. de Salas, D. V. Forero, C. A. Ternes, M. Tortola, and J. W. F. Valle, *Phys.Lett.* **B782**, 633 (2018), arXiv:1708.01186 [hep-ph].
- [24] F. Capozzi, E. Lisi, A. Marrone, and A. Palazzo, *Prog.Part.Nucl.Phys.* **102**, 48 (2018), arXiv:1804.09678 [hep-ph].
- [25] I. Esteban, M. Gonzalez-Garcia, A. Hernandez-Cabezudo, M. Maltoni, and T. Schwetz, *JHEP* **1901**, 106 (2019), arXiv:1811.05487 [hep-ph].
- [26] M. Tanabashi *et al.* (Particle Data Group), *Phys. Rev.* **D98**, 030001 (2018).
- [27] P. F. de Salas, S. Gariazzo, O. Mena, C. A. Ternes, and M. Tortola, *Front.Astron.Space Sci.* **5**, 36 (2018), arXiv:1806.11051 [hep-ph].
- [28] C. Giunti, Y. F. Li, B. R. Littlejohn, and P. T. Surukuchi, *Phys.Rev.* **D99**, 073005 (2019), arXiv:1901.01807 [hep-ph].
- [29] J. Berryman and P. Huber, *Phys.Rev.* **D101**, 015008 (2020), arXiv:1909.09267 [hep-ph].
- [30] C. Giunti, M. Laveder, Y. F. Li, Q. Liu, and H. Long, *Phys. Rev.* **D86**, 113014 (2012), arXiv:1210.5715 [hep-ph].
- [31] B. Achkar *et al.* (Bugey), *Nucl. Phys.* **B434**, 503 (1995).
- [32] J. Kopp, P. A. N. Machado, M. Maltoni, and T. Schwetz, *JHEP* **1305**, 050 (2013), arXiv:1303.3011 [hep-ph].
- [33] I. Alekseev *et al.* (DANSS), *Phys.Lett.* **B787**, 56 (2018), arXiv:1804.04046 [hep-ex].
- [34] M. Danilov (DANSS), arXiv:1911.10140 [hep-ex].
- [35] J. Ashenfelter *et al.* (PROSPECT), *Phys.Rev.Lett.* **121**, 251802 (2018), arXiv:1806.02784 [hep-ex].
- [36] H. Almazan *et al.* (STEREO), *Phys.Rev.Lett.* **121**,

- 161801 (2018), arXiv:1806.02096 [hep-ex].
- [37] H. Almazan Molina *et al.* (STEREO), arXiv:1912.06582 [hep-ex].
- [38] Y. Ko *et al.* (NEOS), Phys.Rev.Lett. **118**, 121802 (2017), arXiv:1610.05134 [hep-ex].
- [39] F. An *et al.* (Daya Bay), Chin.Phys. **C41**, 013002 (2017), arXiv:1607.05378 [hep-ex].
- [40] S. Gariazzo, C. Giunti, M. Laveder, and Y. F. Li, JHEP **1706**, 135 (2017), arXiv:1703.00860 [hep-ph].
- [41] S. Gariazzo, C. Giunti, M. Laveder, and Y. F. Li, Phys.Lett. **B782**, 13 (2018), arXiv:1801.06467 [hep-ph].
- [42] M. Dentler, A. Hernandez-Cabezudo, J. Kopp, P. A. N. Machado, M. Maltoni, I. Martinez-Soler, and T. Schwetz, JHEP **1808**, 010 (2018), arXiv:1803.10661 [hep-ph].
- [43] S.-H. Seo (RENO), AIP Conf. Proc. **1666**, 080002 (2015), arXiv:1410.7987 [hep-ex].
- [44] J. Choi *et al.* (RENO), Phys. Rev. Lett. **116**, 211801 (2016), arXiv:1511.05849 [hep-ex].
- [45] Y. Abe *et al.* (Double Chooz), JHEP **10**, 086 (2014), [Erratum: JHEP 02, 074 (2015)], arXiv:1406.7763 [hep-ex].
- [46] P. Huber, Nucl. Phys. **B908**, 268 (2016), arXiv:1602.01499 [hep-ph].
- [47] A. C. Hayes and P. Vogel, Ann.Rev.Nucl.Part.Sci. **66**, 219 (2016), arXiv:1605.02047 [hep-ph].
- [48] A. Hayes *et al.*, Phys.Rev.Lett. **120**, 022503 (2018), arXiv:1707.07728 [nucl-th].
- [49] J. N. Bahcall, Phys. Rev. **C56**, 3391 (1997), hep-ph/9710491.
- [50] W. C. Haxton, Phys. Lett. **B431**, 110 (1998), nucl-th/9804011.
- [51] D. Frekers, H. Ejiri, H. Akimune, T. Adachi, B. Bilgier, *et al.*, Phys. Lett. **B706**, 134 (2011).
- [52] J. Kostensalo, J. Suhonen, C. Giunti, and P. C. Srivastava, Phys.Lett. **B795**, 542 (2019), arXiv:1906.10980 [nucl-th].
- [53] J. N. Abdurashitov *et al.* (SAGE), Phys. Rev. **C73**, 045805 (2006), nucl-ex/0512041.
- [54] M. Laveder, Nucl. Phys. Proc. Suppl. **168**, 344 (2007).
- [55] C. Giunti and M. Laveder, Mod. Phys. Lett. **A22**, 2499 (2007), hep-ph/0610352.
- [56] M. A. Acero, C. Giunti, and M. Laveder, Phys. Rev. **D78**, 073009 (2008), arXiv:0711.4222 [hep-ph].
- [57] C. Giunti and M. Laveder, Phys. Rev. **D80**, 013005 (2009), arXiv:0902.1992 [hep-ph].
- [58] C. Giunti and M. Laveder, Phys. Rev. **C83**, 065504 (2011), arXiv:1006.3244 [hep-ph].
- [59] P. Anselmann *et al.* (GALLEX), Phys. Lett. **B342**, 440 (1995).
- [60] W. Hampel *et al.* (GALLEX), Phys. Lett. **B420**, 114 (1998).
- [61] F. Kaether, W. Hampel, G. Heusser, J. Kiko, and T. Kirsten, Phys. Lett. **B685**, 47 (2010), arXiv:1001.2731 [hep-ex].
- [62] J. N. Abdurashitov *et al.* (SAGE), Phys. Rev. Lett. **77**, 4708 (1996).
- [63] J. N. Abdurashitov *et al.* (SAGE), Phys. Rev. **C59**, 2246 (1999), hep-ph/9803418.
- [64] J. N. Abdurashitov *et al.* (SAGE), Phys. Rev. **C80**, 015807 (2009), arXiv:0901.2200 [nucl-ex].
- [65] D. Krofcheck *et al.*, Phys. Rev. Lett. **55**, 1051 (1985).